Electronic Supplementary Material (ESI) for Catalysis Science & Technology.


Supporting Information

# The structural evolution of $Mo_2C$ and $Mo_2C/SiO_2$ under dry reforming of methane conditions: morphology and support effects

Alexey Kurlov,[†a] Dragos Stoian,[b] Ali Baghizadeh,[c] Evgenia Kountoupi,[a] Evgeniya B. Deeva,[a] Marc Willinger,[††c] Paula M. Abdala,[*a] Alexey Fedorov[*a] and Christoph R. Müller[*a]

[a] *ETH Zürich, Department of Mechanical and Process Engineering, Leonhardstrasse 21, CH 8092 Zürich, Switzerland*

[b] *Swiss-Norwegian Beamlines at the European Synchrotron Radiation Facility, 71 Avenue des Martyrs, Grenoble, France*

[c] *ETH Zürich, Scientific Center for Optical and Electron Microscopy, Auguste-Piccard-Hof 1, CH 8093 Zürich, Switzerland*

[†] *Present address: Paul Scherrer Institute, Laboratory for Bioenergy and Catalysis, 5232 Villigen PSI, Switzerland*

[††] *Present address: Department of Chemistry, Technical University Munich, Lichtenbergstrasse 4, 85748 Garching, Munich*

E-mail:

* abdalap@ethz.ch
* fedoroal@ethz.ch
* muelchri@ethz.ch

## List of Figures

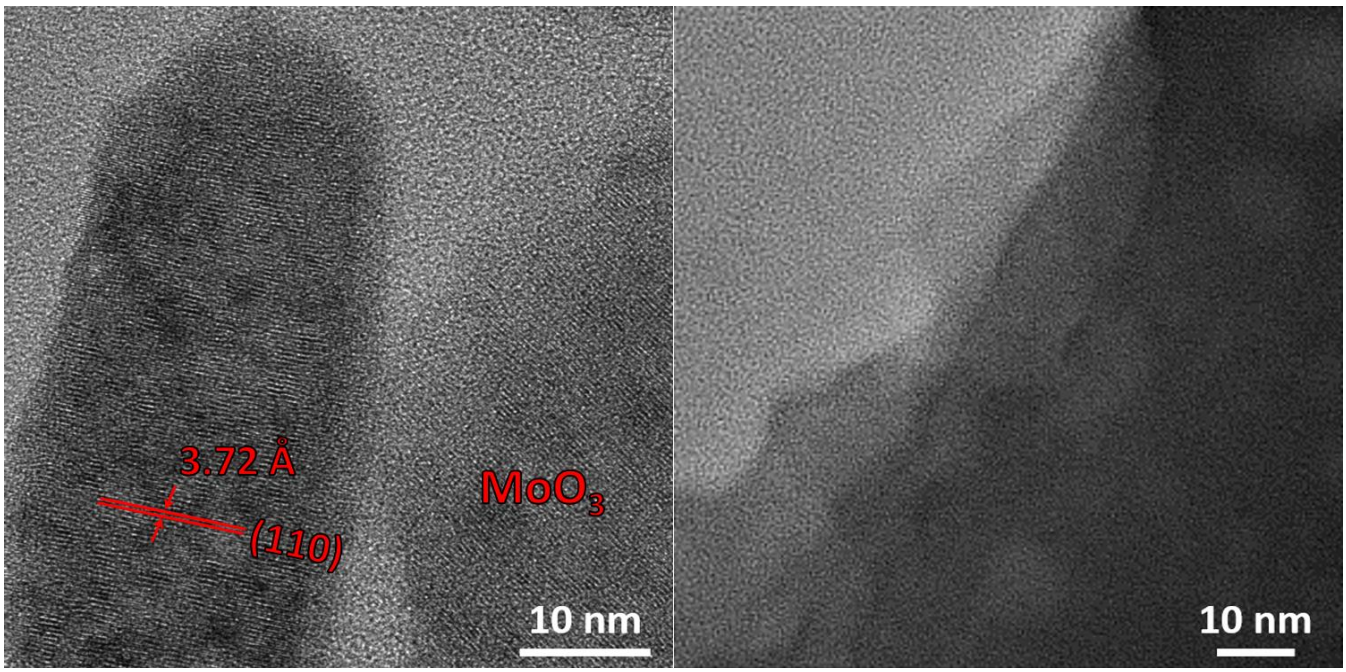


**Figure S1.** TEM images of exfoliated *d*-$MoO_3$.

We note that TEM images of exfoliated *d*-$MoO_3$ have been reported by us previously, see Kurlov et al., *Nanoscale*, **2020**, *12*, 13086–13094, and are reproduced here for completeness and comparison to TEM characterization of $MoO_3/SiO_2$.

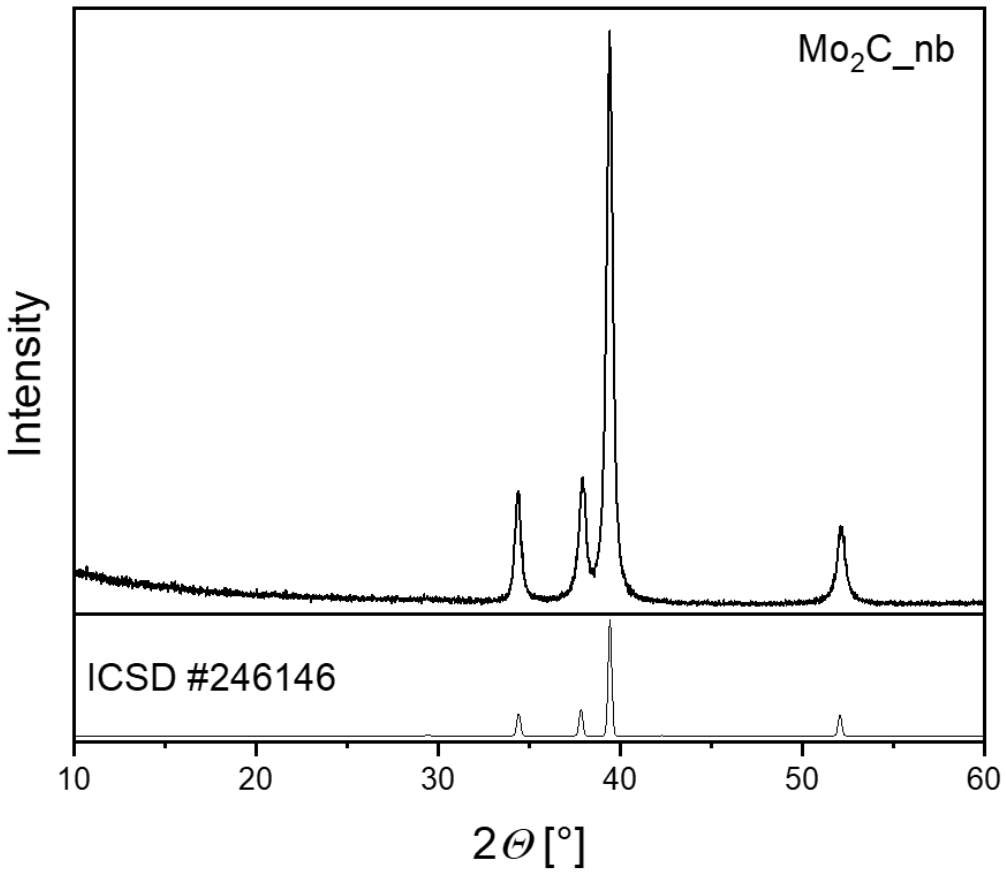


**Figure S2.** XRD pattern of carburized $Mo_2C$-nb and simulated $Mo_2C$ reference pattern (ICSD #246146).

Average crystallite size of $Mo_2C$_nb (determined using the full width at half maximum, FWHM, of the reflection centered at 34.4 in 2Θ) = 26 nm.

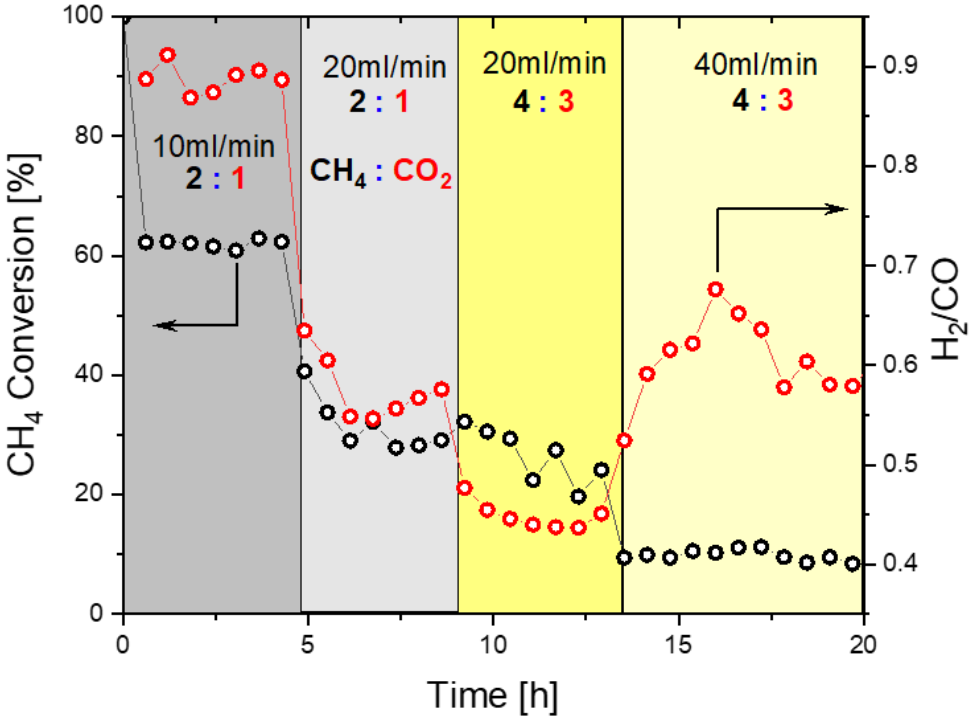


**Figure S3.** Catalytic performance of $Mo_2C$-nb in DRM (laboratory scale reactor, 800 °C, 8 bar, W/F = 75 - 300 ms $g_{Mo}$ $mL^{-1}$).

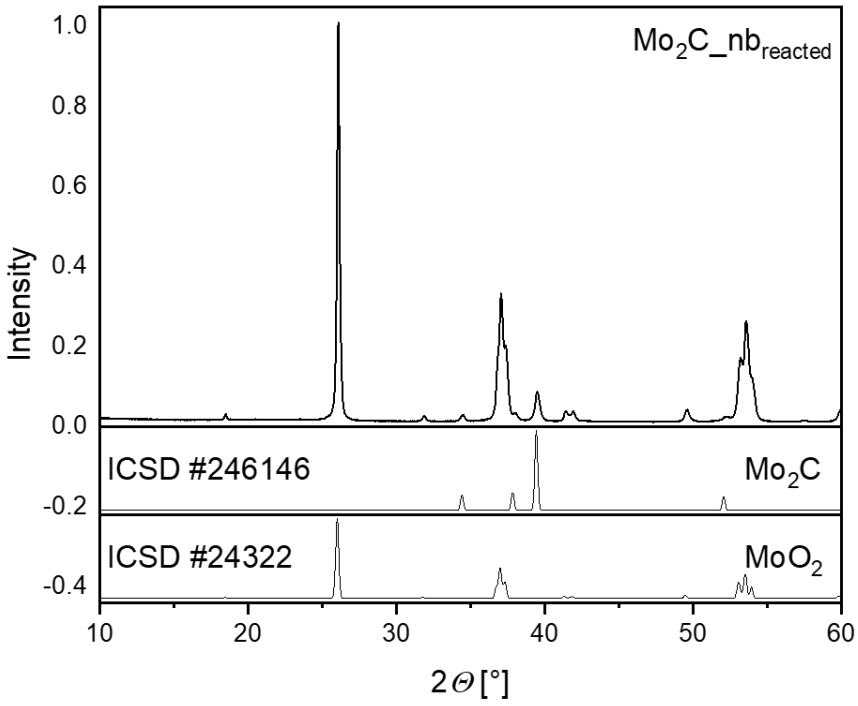


**Figure S4.** XRD pattern of $Mo_2C$-nb after the DRM reaction (as presented in Figure S3) and simulated $Mo_2C$ (ICSD #246146) and $MoO_2$ (ICSD #24322) reference patterns.

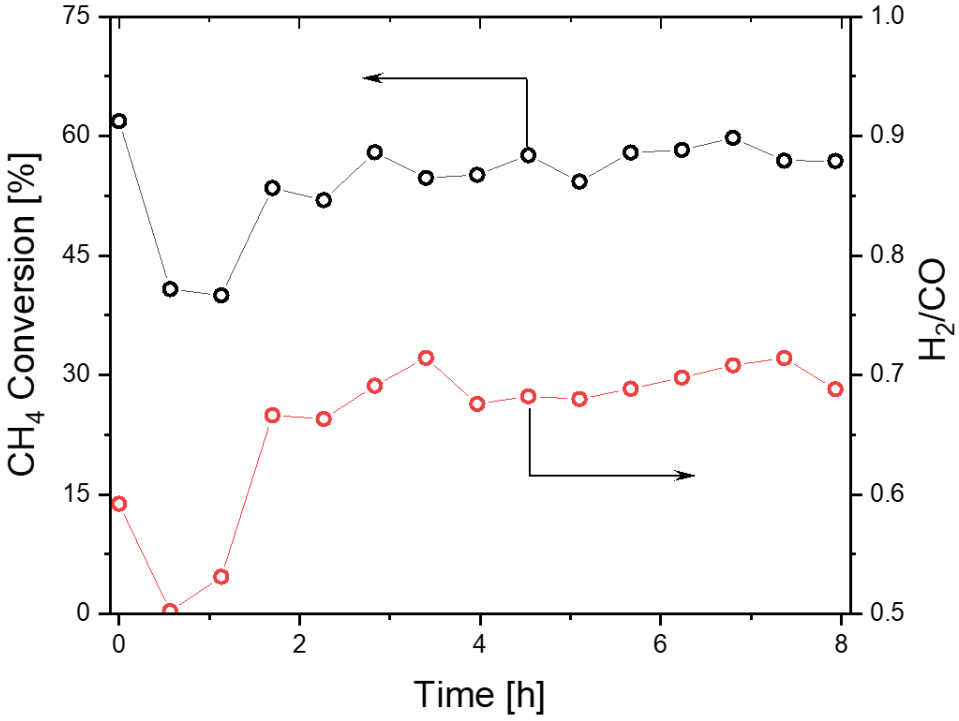


**Figure S5.** Catalytic performance of $Mo_2C/SiO_2$ in DRM (laboratory scale reactor, 800 °C, 8 bar, W/F = 5.25 ms $g_{Mo}$ $mL^{-1}$, $CH_4$ : $CO_2$ : $N_2$ = 4 : 3 : 3).

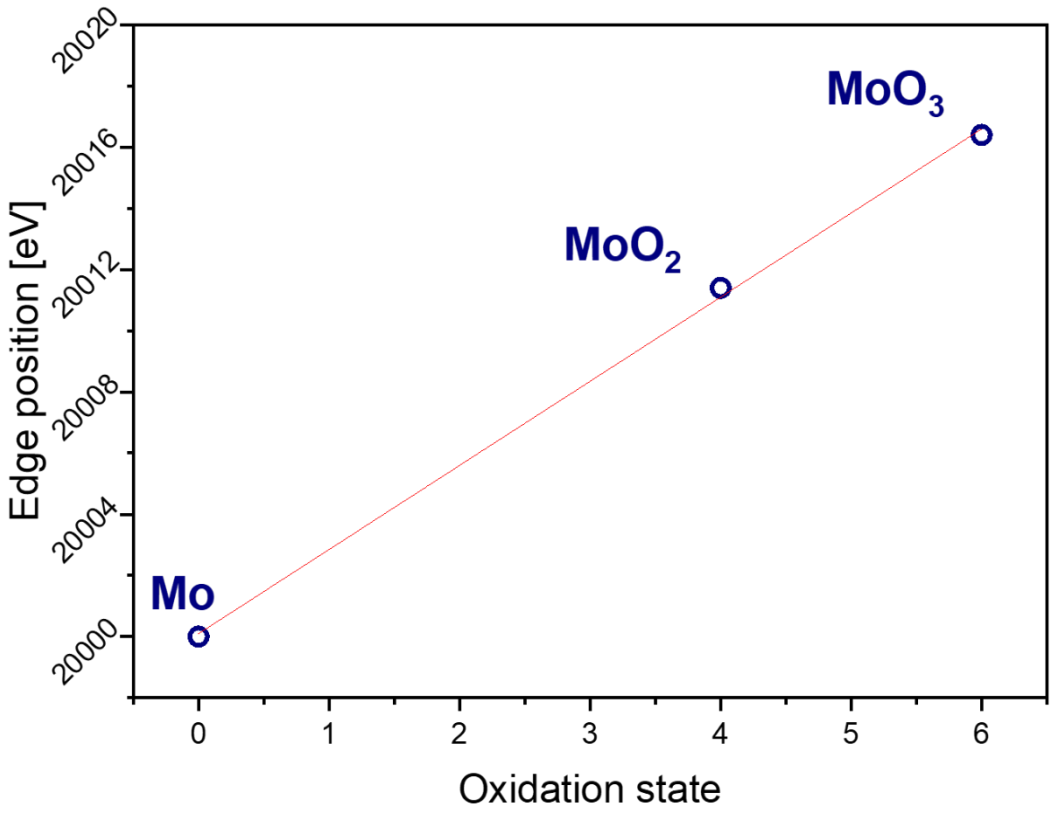


**Figure S6.** Energy edge position of the Mo XANES spectra vs. Mo oxidation state in reference materials.

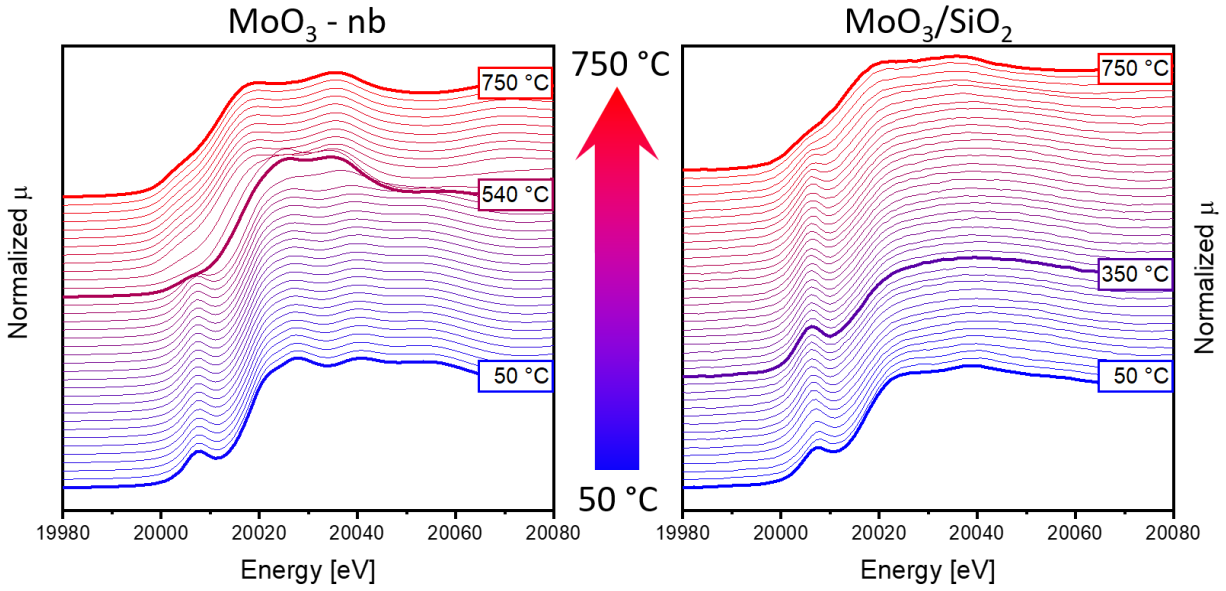


**Figure S7.** In situ carburization of $MoO_3$-nb (left) and $MoO_3/SiO_2$ (right) under $H_2 : CH_4 = 4 : 1$ gas mixture followed by Mo K-edge XANES.

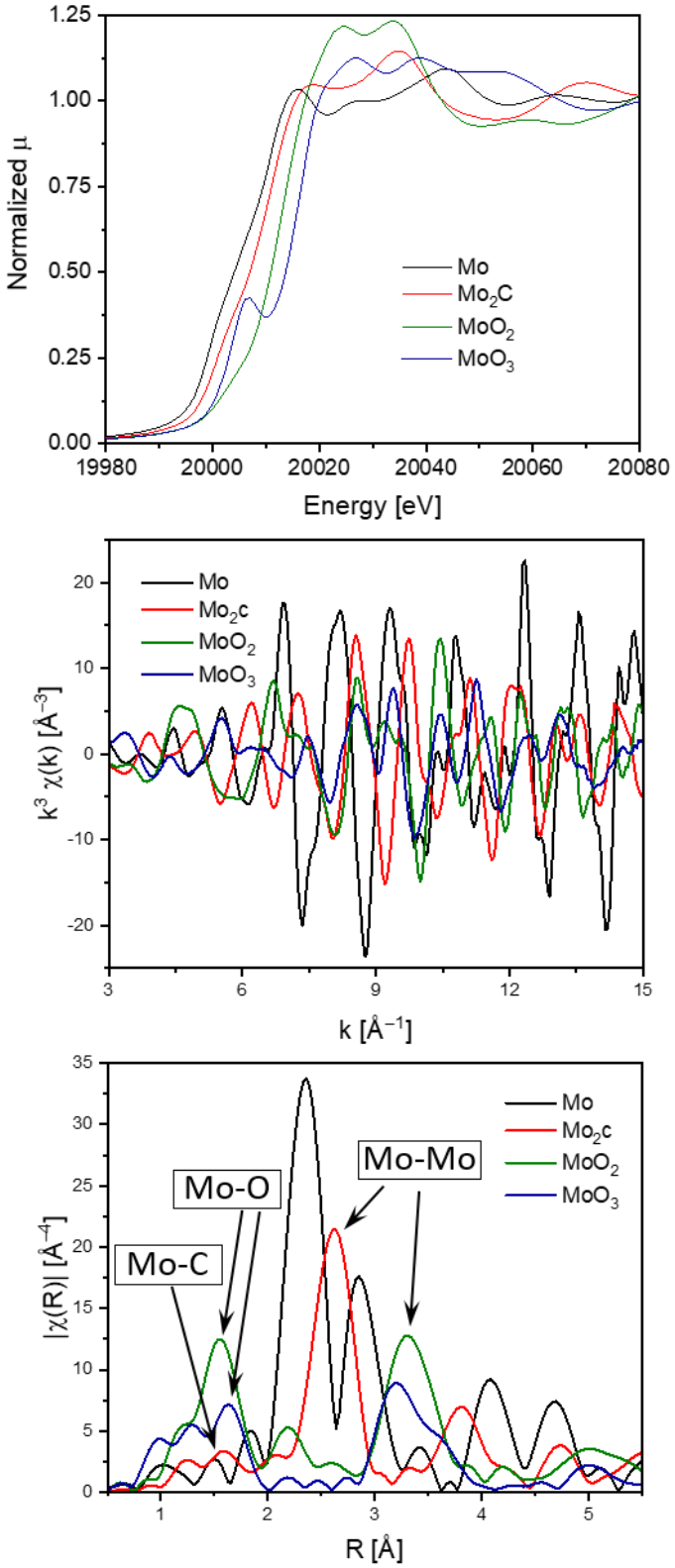


**Figure S8.** Mo K-edge XANES spectra (top), $k^3$ -weighted EXAFS (middle) and (uncorrected for the phase shift) Fourier-transformed EXAFS functions (bottom) of reference materials ($\Delta k = 3 – 15$ Å$^{-1}$).

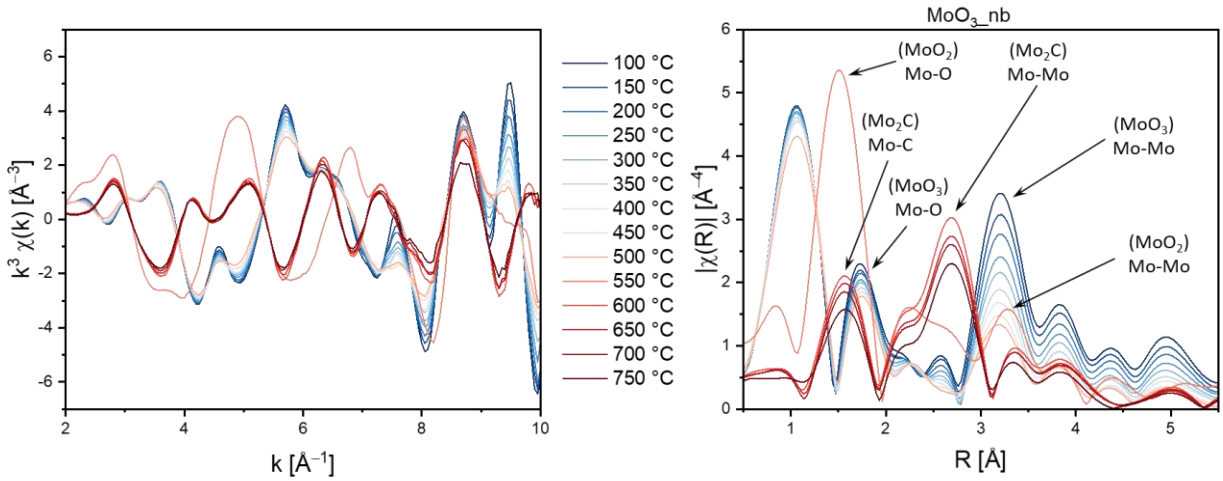


**Figure S9.** *In situ* $k^3$ -weighted EXAFS (left) and the corresponding Fourier-transform (right) for $MoO_3$-nb during carburization. ($\Delta k = 3 - 10$ Å$^{-1}$)

At ca. 600 °C Mo-C and Mo-Mo peaks at 1-2 Å and 2-3 Å appear in the (non-phase corrected) EXAFS Fourier-transform data, in line with the formation of a $Mo_2C$ phase. Due to the high thermal disorder in the EXAFS signal no quantitative information could be extracted, yet it can be observed that the changes in the EXAFS data qualitatively agree with the XANES analysis.

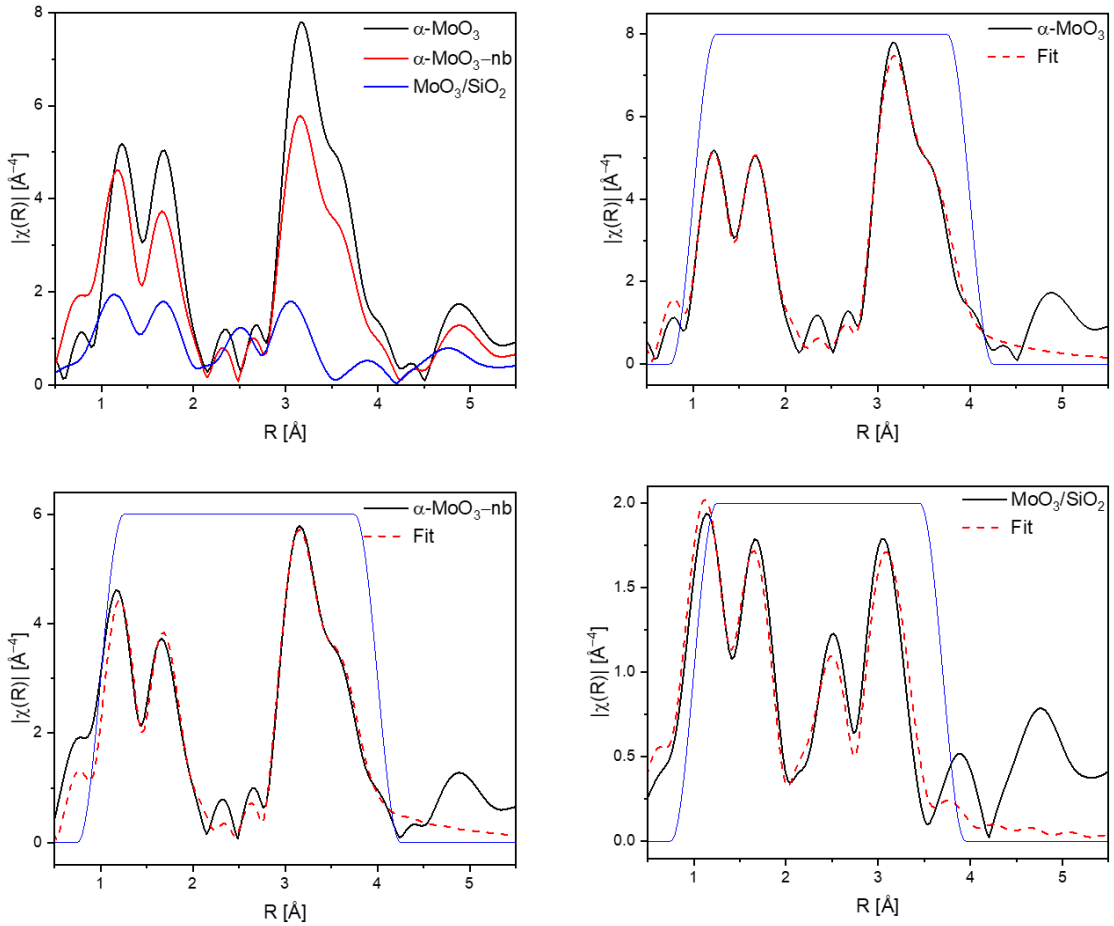


**Figure S10.** Comparison of Fourier-transformed EXAFS functions and EXAFS fittings of α-$MoO_3$, α-$MoO_3$-nb and $MoO_3/SiO_2$. ($\Delta k = 3 - 10$ Å$^{-1}$).

**Table S1. EXAFS fitting of reference $MoO_3$, α-$MoO_3$-nb and $MoO_3/SiO_2$.**

Description of the fitting procedure. EXAFS fittings were performed in R-space with $\Delta k = 3 – 10$ Å$^{-1}$ and $\Delta R = 1 – 4$ Å. The amplitude reduction factor $S_0$ was determined to be 1 from the fitting of the α-$MoO_3$ reference.
The fittings for the α-$MoO_3$ reference and α-$MoO_3$-nb were performed using a local structure model based on the crystallographic structure of α-$MoO_3$, with fixed coordination numbers (CN), free interatomic distances R, while the Debye–Waller factors i.e., the variance of the distance distribution ($\sigma^2$), were determined and restrained to be the same for all the Mo-O and Mo-Mo paths. This model fitting used 9 variable of 13 independent points.
For $MoO_3/SiO_2$, the α-$MoO_3$ model was not applicable, and the best fit was obtained when using two Mo-O spheres, one Mo-Si and one Mo-M sphere, with varying CN. We also tested a local structure model for $MoO_3/SiO_2$ without including the Mo-Si path, yet the agreement factor (R-factor) was above 0.2, demonstrating that a Mo-Si path was needed to account for the local structure of this material. This model fitting used 9 variable of 13 independent points.

**Reference α-$MoO_3$ (R-factor 0.005)**

| Shell | CN | R (Å) | $\sigma^2$ (Å$^2$) | ΔE (eV) |
|---|---|---|---|---|
| Mo — $O_1$ | 2 | 1.71 (1) | 0.003 (1) | 5 (1) |
| Mo — $O_2$ | 2 | 1.97 (1) | 0.003 (1) | |
| Mo — $O_3$ | 1 | 2.31 (1) | 0.003 (1) | |
| Mo — $Mo_1$ | 2 | 3.45 (1) | 0.003 (1) | |
| Mo — $Mo_2$ | 2 | 3.83 (3) | 0.003 (1) | |
| Mo — $Mo_3$ | 2 | 3.98 (1) | 0.003 (1) | |

**α-$MoO_3$-nb (R-factor 0.017)**

| Shell | CN | R (Å) | $\sigma^2$ (Å$^2$) | ΔE (eV) |
|---|---|---|---|---|
| Mo — $O_1$ | 2 | 1.71 (1) | 0.004 (1) | 3 (1) |
| Mo — $O_2$ | 2 | 1.96 (1) | 0.004 (1) | |
| Mo — $O_3$ | 1 | 2.29 (2) | 0.004 (1) | |
| Mo — $Mo_1$ | 2 | 3.44 (1) | 0.004 (1) | |
| Mo — $Mo_2$ | 2 | 3.70 (3) | 0.004 (1) | |
| Mo — $Mo_3$ | 2 | 3.96 (1) | 0.004 (1) | |

**$MoO_3/SiO_2$ (R-factor 0.015)**

| Shell | CN | R (Å) | $\sigma^2$ (Å$^2$) | ΔE (eV) |
|---|---|---|---|---|
| Mo — $O_1$ | 2 (1) | 1.75 (2) | 0.012 (5) | 7 (1) |
| Mo — $O_2$ | 3 (1) | 1.98 (2) | 0.012 (5) | |
| Mo — $Si_1$ | 0.6 (4) | 2.7 (5) | 0.010 (4) | |
| Mo — $Mo_1$ | 3 (2) | 3.41 (1) | 0.010 (4) | |

**$MoO_3/SiO_2$ without Mo-Si (R-factor 0.027)**

| Shell | CN | R (Å) | $\sigma^2$ (Å$^2$) | ΔE (eV) |
|---|---|---|---|---|
| Mo — $O_1$ | 2 (1) | 1.75 (2) | 0.010 (5) | 6 (1) |
| Mo — $O_2$ | 2 (1) | 1.98 (2) | 0.010 (5) | |
| Mo — $Mo_1$ | 3 (2) | 3.41 (1) | 0.011(4) | |

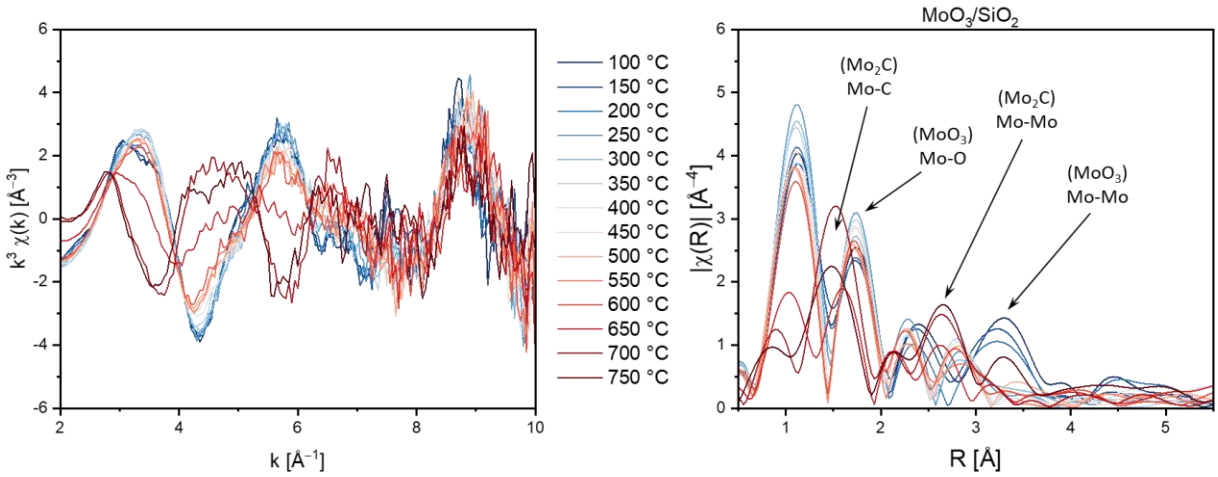


**Figure S11.** *In situ* $k^3$ -weighted EXAFS (left) and the corresponding Fourier-transform (right) for $MoO_3/SiO_2$ during its carburization. ($\Delta k = 3 - 10$ Å$^{-1}$)

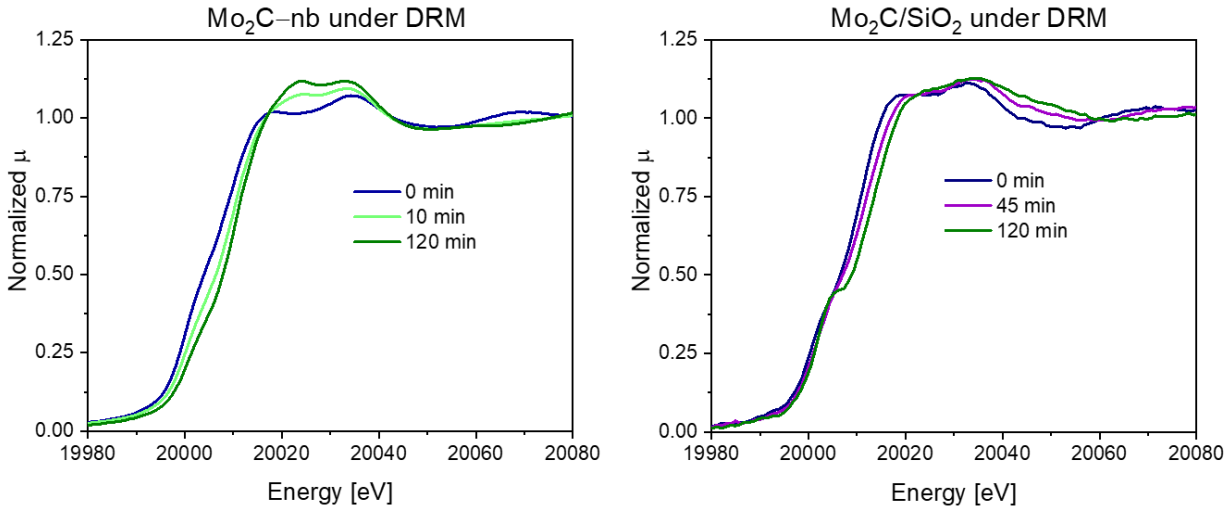


**Figure S12.** Comparison of individual Mo K-edge spectra of $Mo_2C$-nb (left) and $Mo_2C/SiO_2$ (right) at different stages in the DRM reaction.

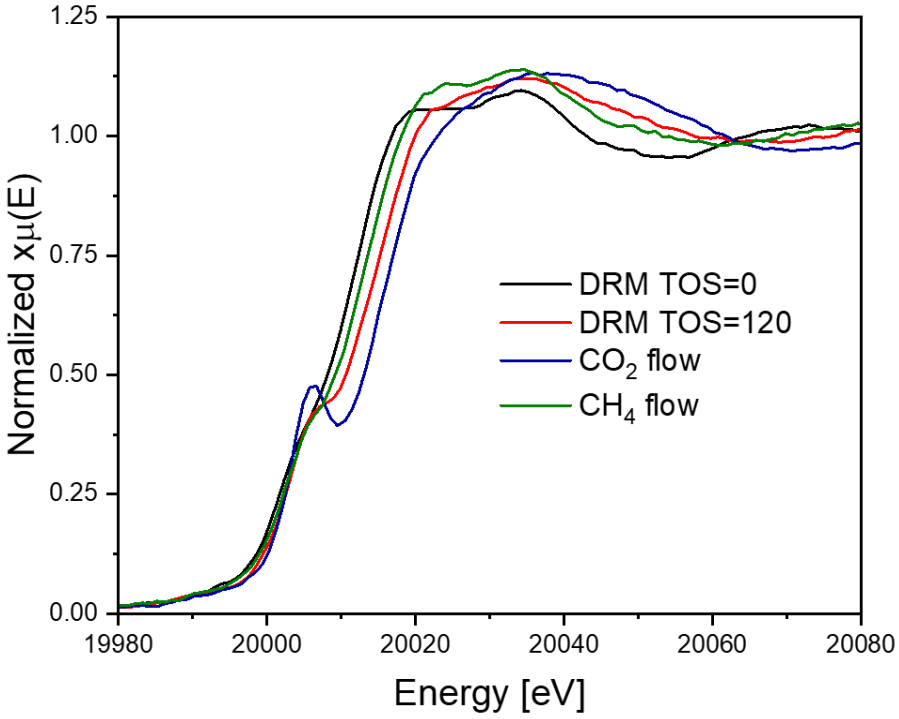


**Figure S13.** Comparison of individual Mo K-edge spectra of $Mo_2C/SiO_2$ after TOS = 0 and 120 min, with a subsequent exposure to a $CO_2$ flow, and then to a $CH_4$ flow.

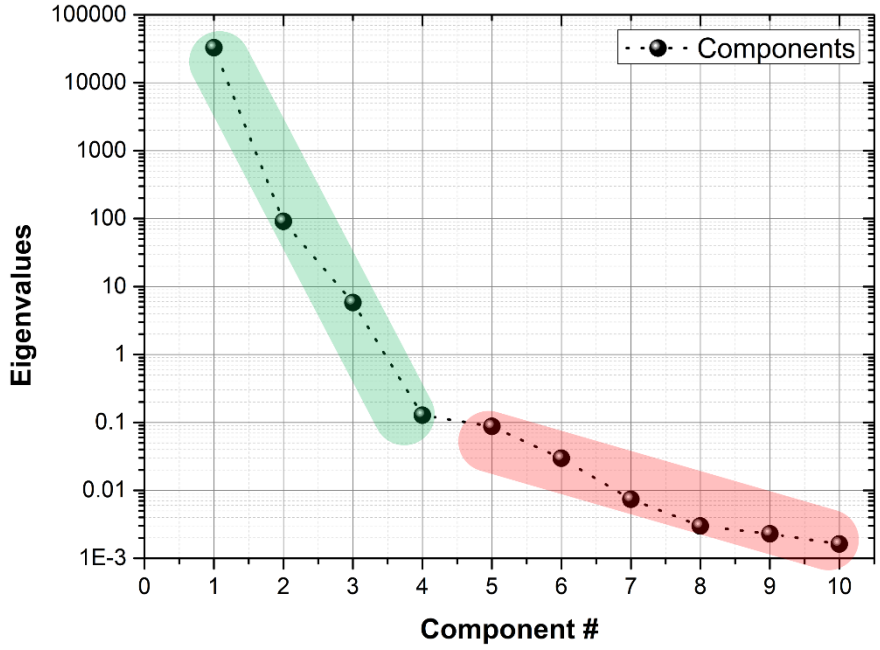


**Figure S14.** PCA analysis of $MoO_3$-nb.

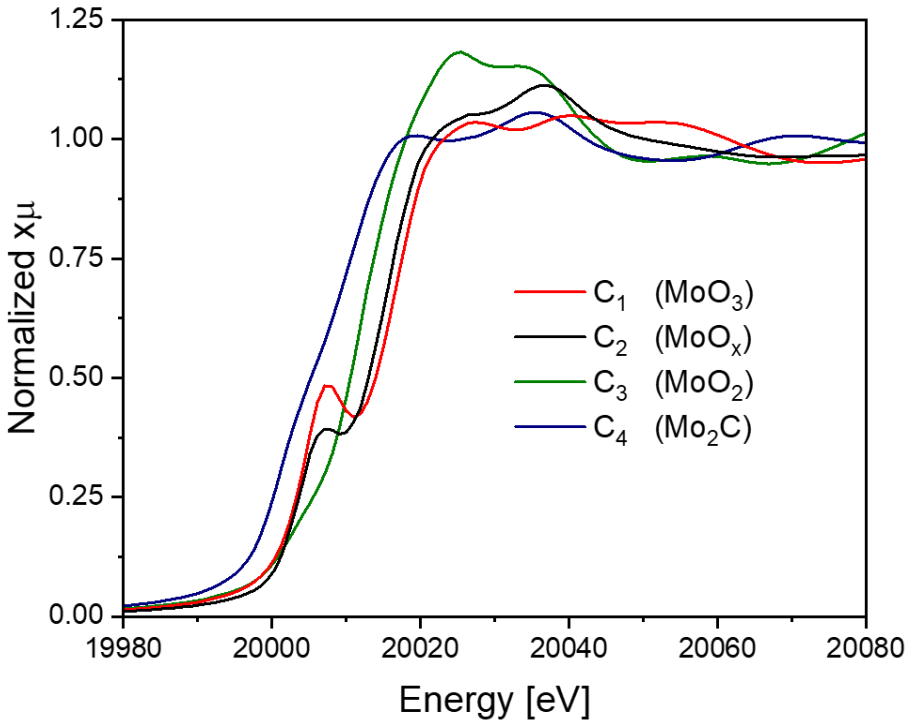


**Figure S15.** Theoretical XANES spectra of the components obtained by MCR-ALS analysis during the carburization of α-$MoO_3$-nb.

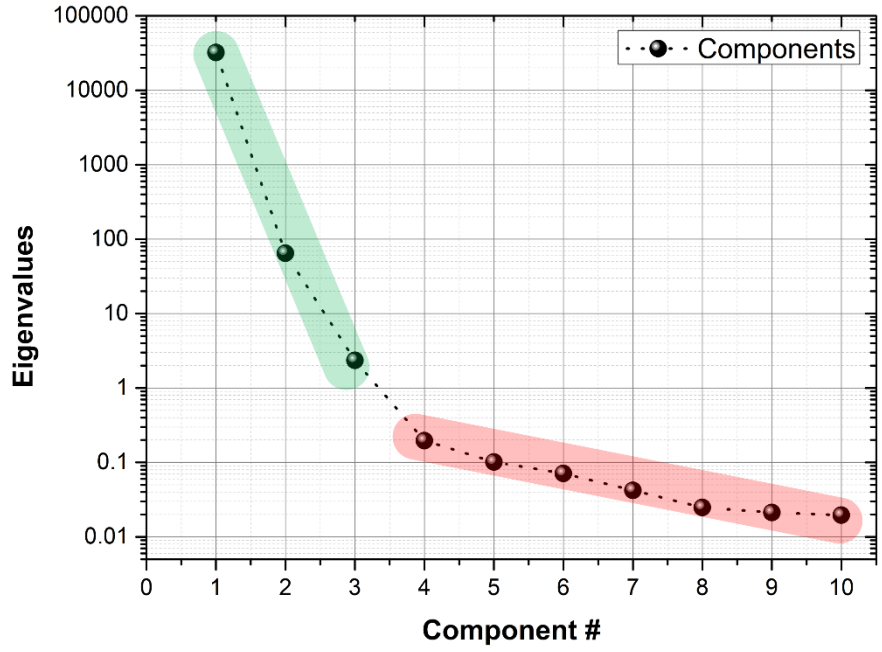


**Figure S16.** PCA analysis of $MoO_3/SiO_2$.

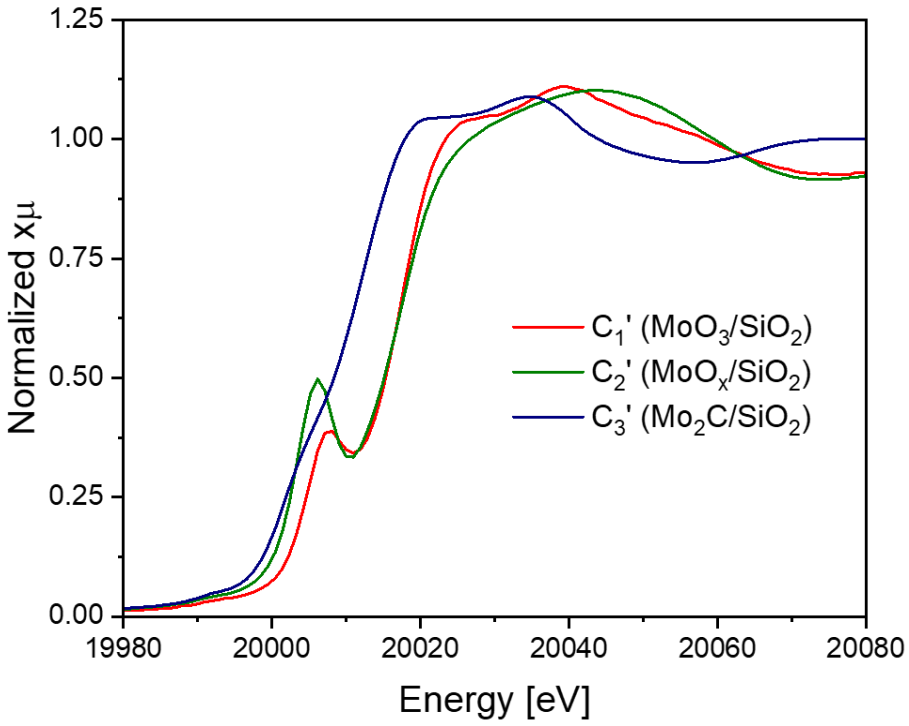


**Figure S17.** Theoretical XANES spectra of the components obtained by MCR-ALS analysis during the carburization of $MoO_3/SiO_2$.

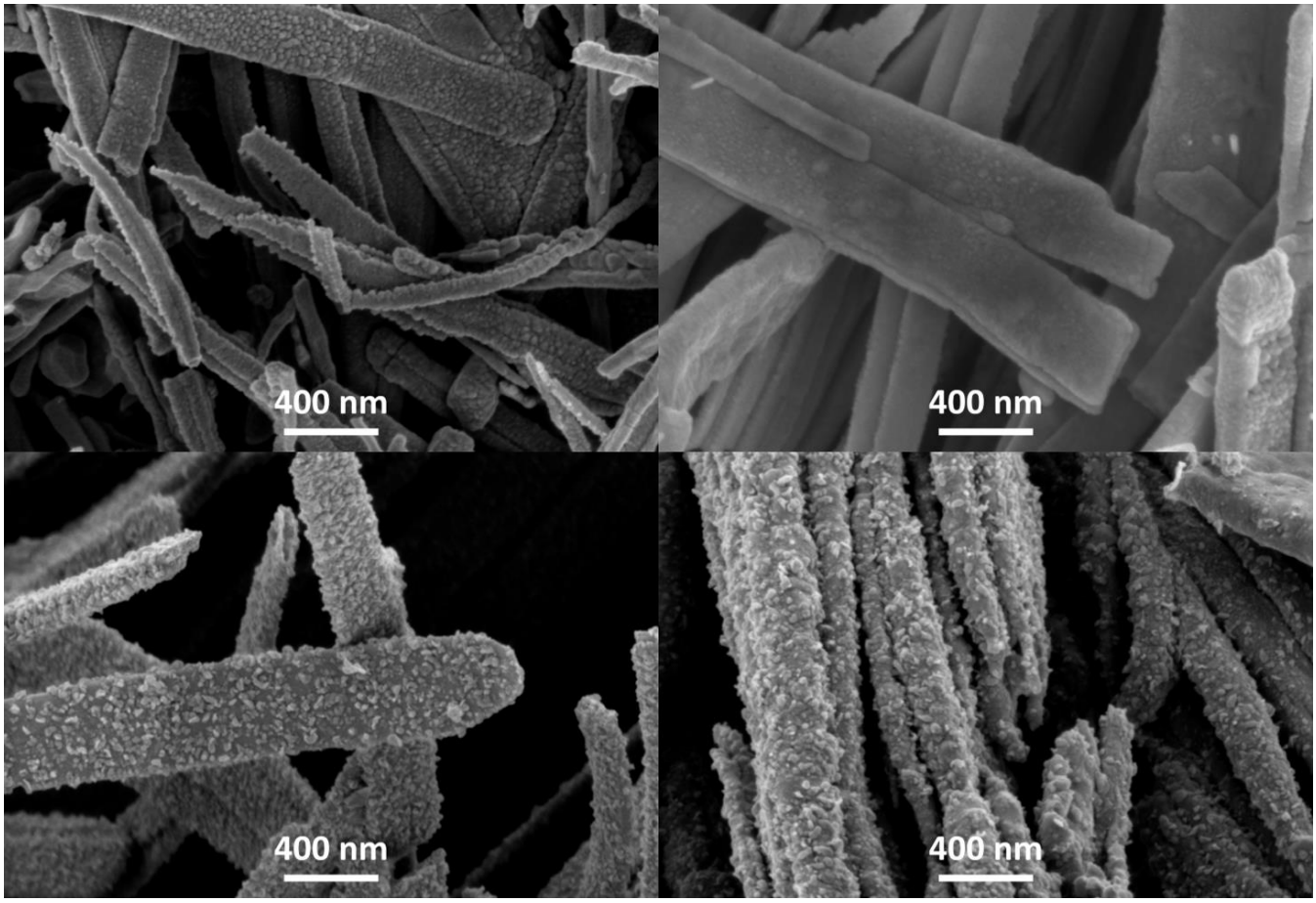


**Figure S18.** SEM images of $Mo_2C$-nb after the DRM reaction.

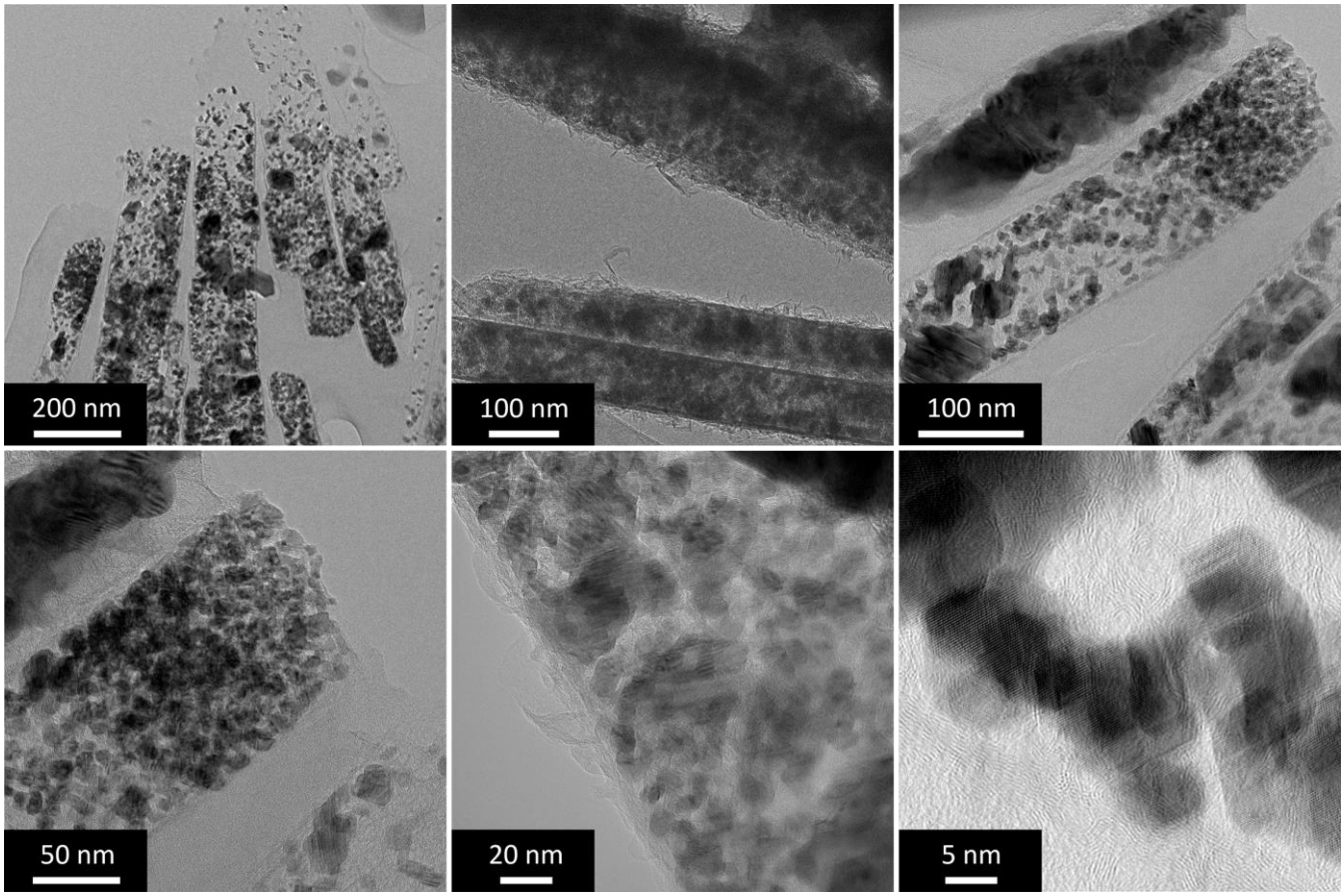


**Figure S19.** TEM images of a $Mo_2C$-nb cross-section after the DRM reaction revealing a heterogeneous porous structure.

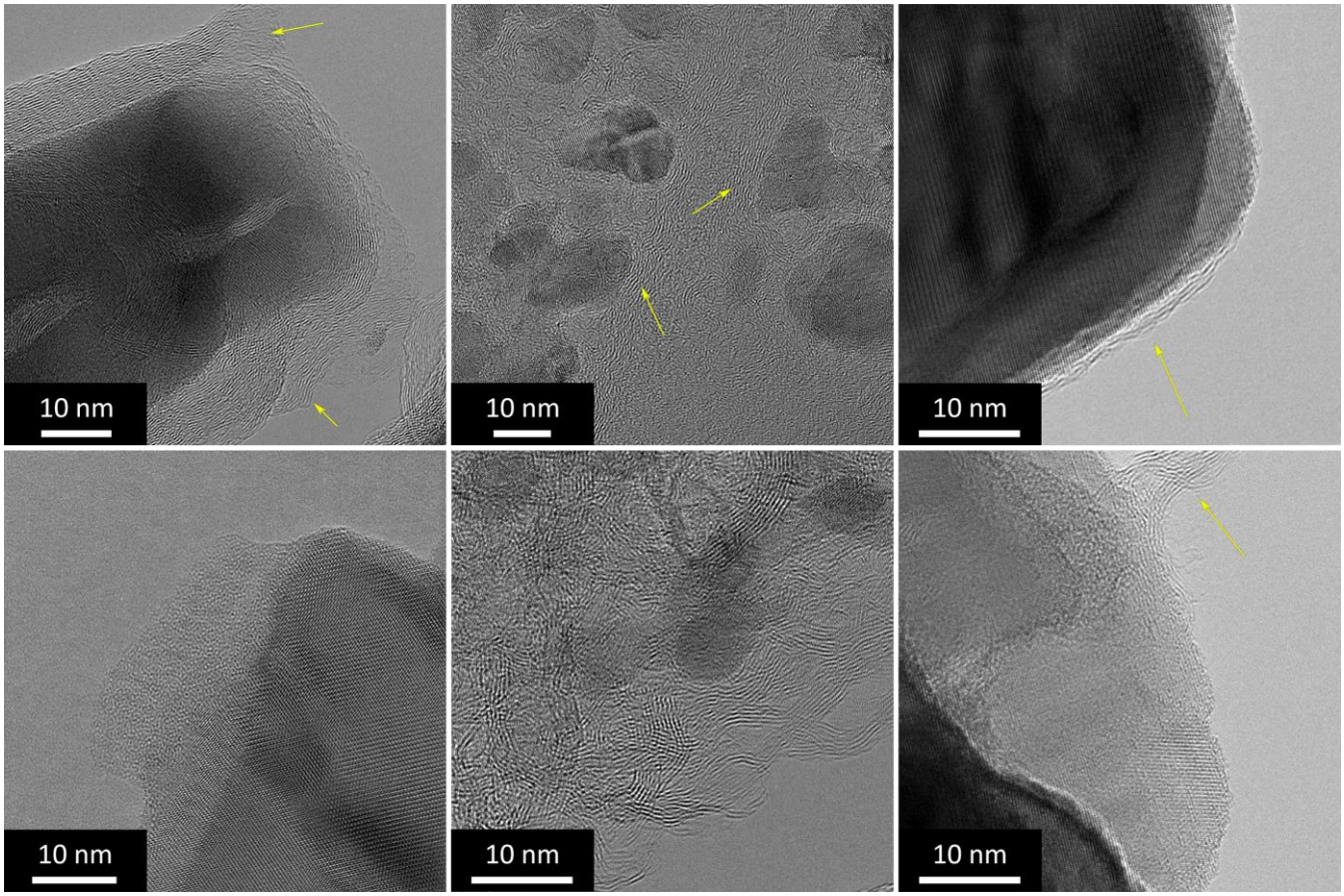


**Figure S20.** TEM images of a $Mo_2C$-nb cross-section after the DRM reaction revealing graphitic and/or carbon covering the surface of the nanoparticles. The arrows point at the graphitic layers around the used $Mo_2C$-nb.